J. Fluid Mech. (1989), *vol.* 205, *pp.* 171–193
Printed in Great Britain

Measurement of turbulent dispersion behind a fine cylindrical heat source in a weakly sheared flow

By MYUNG KYOON CHUNG[1] AND NAM HO KYONG[2]

[1] Korea Advanced Institute of Science and Technology, Seoul, Korea

[2] Korea Institute of Energy and Resources, Daeduck, Korea

(Received 1 May 1987 and in revised form 3 January 1989)

Turbulent structure in a turbulent scalar dispersion field behind a fine cylindrical heat source in a weakly sheared flow is experimentally investigated and previous computational turbulence models for third-order scalar transport terms in the second-order turbulence equations are assessed with the present data.

The mean temperature and r.m.s. temperature profiles are found to be almost Gaussian even in the uniform shear layer. Decay of the peak temperature, mean dispersion and half-widths of the mean temperature and the r.m.s. temperatures are well correlated with corresponding data on the scalar dispersion behind an elevated line heat source in the turbulent boundary layer.

Normalized streamwise heat flux $\overline{u\theta}$ changes appreciably with the downstream distance owing to the influence of the uniform mean shear, whereas normalized vertical heat flux $\overline{v\theta}$ remains the same with the downstream distance. The timescale ratio R between temperature and velocity fluctuations varies from 0.3 to 1.3 across the stream and it asymptotes to a value 0.5 at far downstream.

Assessment of previous models for third-order moments with the present data reveals that application of a composite timescale between the dynamic timescale and the thermal timescale to the simplest gradient transport model yields a better overall prediction performance than any existing models, including Lumley's algebraic model equations for the moments. It was found that the timescale for the streamwise transports of $\overline{u\theta}$ and $\overline{\theta^2}$ is larger than that of lateral transports of $\overline{v\theta}$ and $\overline{\theta^2}$.

In addition, since the experiment isolates the effect of uniform mean shear on the turbulent scalar transport, experimental data accumulated by the present study will be useful for further development of more refined second-order turbulence models for non-isothermal turbulent flows.

1. Introduction

Since the Reynolds stress closure model for isothermal turbulent flows was established in the mid-1970s, turbulent transports of scalar quantities, be it temperature, humidity, a pollutant or any other chemical, have attracted the attention of theoretical and experimental investigators. As with the modelling procedure for isothermal turbulent flows (as has been well-documented by Reynolds 1976), a systematic way to develop the second-order closure model for the non-isothermal turbulent flow is to consider one turbulence mechanism at a time in order of increasing complexity, for example, in a sequence to determine the decay rate constant of scalar variance, pressure–temperature gradient correlation or the return-to-isotropy of the scalar flux vector and then third-order scalar transports. At each

stage of modelling, the simplest experiments which exhibit only the mechanism under consideration must be available to calibrate the model constant (or term).

Such a systematic experimental approach to the problem of thermal turbulence has been taken by Warhaft & Lumley (1978) who studied the decaying rate of the passive temperature variance $\overline{\theta^2}$ in approximately isotropic grid-generated turbulence. Based on these data, Newman, Launder & Lumley (1981) proposed a model for the decay rate 'constant' ψ_θ as a function of the mechanical/thermal timescale ratio r $(\equiv (\overline{q^2}/\epsilon)/(\overline{\theta^2}/\epsilon_\theta))$, Reynolds number R_l and anisotropy of turbulence. An important result from these studies is that the timescale ratio r varies in a range 0.6–2.4, and, thus, it is found that the governing equation for the destruction of temperature variance ϵ_θ must be solved to provide the correct variation of r in the computation of the thermal turbulence field.

In order to examine the effect of uniform strain on the evolution of thermal fluctuations, Warhaft (1980) carried out an experiment in which thermal fluctuations generated by an array of heated mandolin wires in a decaying grid-generated turbulence were passed through a four-to-one axisymmetric contraction. The effect of a passive cross-stream temperature gradient on the evolution of temperature variance and the heat flux vector $\overline{u_j\theta}$ was experimentally studied by Sirivat & Warhaft (1983). In addition to the cross-stream mean temperature gradient, Budwig, Tavoularis & Corrsin (1985) superimposed a streamwise mean temperature gradient on a grid-generated isotropic turbulence to investigate the effect of such a gradient field on the evolution of various statistics of thermal turbulence, for example, mean temperature, r.m.s. temperature fluctuations, the turbulent heat transfer correlation coefficient, the thermal Taylor microscale λ_θ, and the skewness of the temperature fluctuation derivatives. Tavoularis & Corrsin (1981) measured several moments, spectra, lengthscales, timescales and probability density functions in nearly homogeneous turbulent flow with a uniform mean temperature gradient to study detailed behaviour of thermal turbulence under the influence of the uniform velocity gradient. With the data from Sirivat & Warhaft (1983), Shih & Lumley (1986) have recently formulated a return-to-isotropy model 'constant' ϕ_θ appearing in a scalar flux equation $\overline{u_j\theta}$.

An experiment on the triple product between velocity and temperature (or the third-order scalar transport terms), for example $\overline{u_i u_j u_k}$, $\overline{u_i u_j \theta}$ and $\overline{u_j \theta^2}$, has been carried out by Fabris (1983) who obtained data of all scalar transport terms in a two-dimensional turbulent wake behind a heated circular bar whose diameter was 0.6 mm. Dekeyser & Launder (1985) measured all the scalar transport terms in a heated asymmetric two-dimensional turbulent jet. In addition to the presentation of the data, they carried out numerical tests of currently available gradient-diffusion type models for the scalar triple products against their data. As a result, they showed that the simple gradient-diffusion model cannot consistently predict the scalar triple products in the whole downstream range of measurement, and they suggested that a theoretical model of Lumley (1978) for the scalar transport terms would be worth examining to see if such an extensive, but highly complicated, model would give a better prediction. Raupach & Legg (1983) obtained quite complete turbulence correlations of first-, second- and third-orders behind an elevated line heat source in a turbulent boundary layer. In the same work, currently available closure assumptions for various moments were tested against the experiment. Their findings are that: (i) the gradient-diffusion model at the first-order predicts correctly the turbulent heat flux correlations $\overline{u_j\theta}$, (ii) the turbulence-interaction component of the pressure term requires different timescales for $\overline{u\theta}$ and $\overline{v\theta}$ correlations, and (iii) the

triple products are not well represented by current simple gradient-diffusion models. Unlike the simple gradient-diffusion model (Launder 1978), Zeman & Lumley (1979) and Lumley (1978) have formulated a system of linear equations for nine scalar triple products as unknowns. The coefficient matrix consists of second-order moments and the mean temperature gradient and the elements of the column matrix in the right-hand side are gradients of the second-order moments.

The objectives of the present paper are to study the evolution process of the turbulent thermal structure behind a fine cylindrical heat source in a uniform shear flow and to test the various computational models for the third-order scalar transports. With this in mind, mean field characteristics and higher-order statistical moments are measured in the turbulence field behind the cylindrical heat source in a grid-generated turbulence of uniform mean shear. The experimental details are given in the following section. It is believed that the present experiment is a logical addition to the series of previous experimental works on thermal turbulence.

2. Experimental facilities and instrumentation

2.1. *Wind tunnel of uniform mean shear and a fine cylindrical heat source*

An open-return wind tunnel, 0.6 m × 0.6 m in cross-section and of effective working section 8 m long, was specially designed for this study from the design guide of Mehta & Bradshaw (1979). The wind tunnel was driven by a forward facing multiblade fan powered by a variable speed 15 h.p. motor. The contraction ratio was 9:1 and the maximum attainable speed was 25 m/s with a turbulence intensity of less than 0.3 %. In order to restore the static pressure loss due to friction, both sidewalls of the duct were adjusted at a diffusing angle of about 0.3° for a mean speed of 10 m/s. The contraction nozzle was formed by two cubic arcs and the exit part of the nozzle was carefully trimmed.

The configuration of the shear generator is such that the channel is vertically divided by 14 thin steel plates equally spaced in order to have 15 narrow channels. Two perforated steel bands with equally spaced rectangular holes are folded together at the upstream entrance of each channel. By sliding one steel band over the other, the opening area ratio can be adjusted easily between 0.288 and 0.70. In order to decrease the scale of turbulence at the exit of the shear generator, which is of the order of the channel height 4 cm, a cylindrical rod of diameter 8 mm was installed at the centre of each channel exit. Such an arrangement also helps to obtain better horizontal uniformity of the flow. The uniformity of the shear rate across the test section was tested with a vertically oriented rake of 26 dynamic pressure probes made of 2.12 mm diameter stainless steel tubes. In order to minimize the flow disturbance due to the probes the vertical distances between the probes were set at 2 cm, and the distance between the probe hole and the back stem of the rake was 50 tube diameters (Pope & Harper 1966).

The total pressure signals from the rake and the static pressure signals from wall pressure taps at the same distance x were scanned by a Scanivalve system which consists of a pressure transducer, J-type Scannivalve (SCANCO) and a solenoid controller. Fine adjustment of the shear generator was performed by measuring the local velocity with a single hot-wire probe of platinum-coated tungsten 1.2 mm long and 5 μm diameter. The probe was vertically scanned with a precision traversing mechanism driven by a stepper motor whose movement was controlled by pulse signals from a microcomputer (Commodore PET 4032). The minimum stepping increment was 0.125 mm. A fine stainless steel screen with a square mesh of 1.06 mm

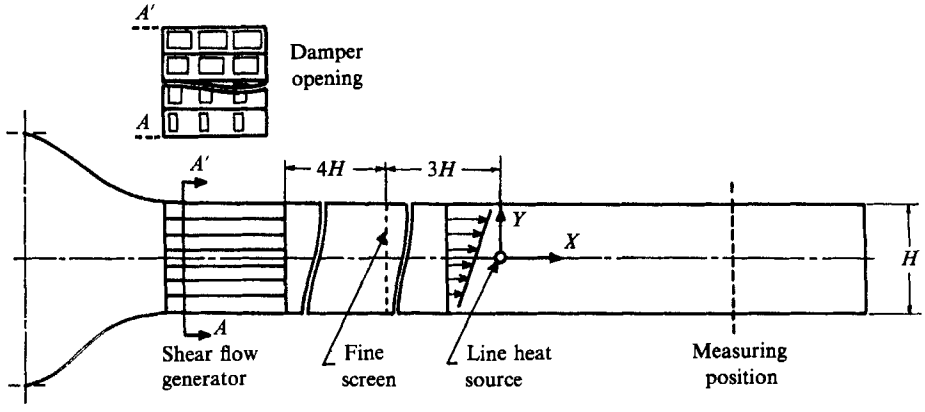

FIGURE 1. Arrangement of a shear generator, fine screen and a heat source in a low-speed wind tunnel.

and solidity of 19% was inserted into the wind tunnel at $x/H = 4$ (here, $H = 0.6$ m is the height of the test section) downstream of the shear generator exit to further reduce the free-stream turbulence and to obtain more uniform shear flow.

As a heat source, a 0.8 mm diameter Ni–Cr wire was stretched horizontally across the test section at $x/H = 7$ and at the centre of the channel height. The wire was heated electrically with an a.c. supply and the power consumption was monitored by a precision wattmeter. Variation of the power consumption during the experiment was within 2%. The temperature of the incoming air to the heating wire was 21.5 ± 0.2 °C. Sagging of the wire owing to wire heating was prevented by giving tension force through the wire by suspending a weight of 1 kg at one end of it. The wire was supported by a pair of Duralumin junctions at both ends. Figure 1 shows the experimental configuration and the front view of the shear generator.

2.2. *Instrumentation and data acquisition*

The streamwise and vertical velocity components and the fluctuation temperature were simultaneously measured by a combination of a constant temperature X-wire probe (TSI, model 1241) and a cold wire. The X-wire was made of platinum wire of diameter 6 μm and length 1.25 mm. The wire overheat ratio was 2.0 and the frequency response was set at 15 kHz. The probe was calibrated with the Collis and William's law, and yaw tested which gave $\psi_1 = 42.3°$ and $\psi_2 = 45.8°$.

The cold wire for the fluctuating temperature measurements was 0.6 μm platinum Wollaston wire and its effective length was 0.3 mm ($1/d = 500$). It was operated as a resistance thermometer in a constant current circuit of 120 A. The frequency response of the cold wire was 6 kHz which was determined by using a pulsed two-wire technique described in Antonia, Browne & Chambers (1981). The resistance-temperature coefficient α was measured to be $\alpha = 0.0035 \pm 0.0001$/K which is the same as LaRue, Deaton & Gibson (1975).

The cold wire was vertically oriented and located 2 mm laterally away from the X-probe. Since the flow has a fluctuating temperature component, the signals from the X-probe were contaminated by the temperature. The two signals were separated by using a method which is described in Subramanian (1980) and Subramanian & Antonia (1981). The cold-wire signal was amplified with a gain of 10^4–10^5 and then low-pass filtered at 10 kHz cut-off. The r.m.s. noise of the cold-wire signal was

0.05 K and the smallest detectable temperature variation was 0.005 K. All signals were recorded on an FM magnetic tape recorder (HP model 3968A, frequency response of 5 kHz) and subsequently digitized by a universal waveform analyser (Data Precision, D-6000). The A/D conversion was done with 14-bit resolution at 10 kHz sampling.

The lateral resolution of our combination probe is about three times larger than the Kolmogorov's microscale, owing to the 2 mm gap between the cold wire and the hot wire. The probe is thus inappropriate for the investigation of small-scale turbulence. However, it is sufficiently small for the measurement of the cross-correlation between the velocity and the temperature which is related to the large-scale turbulence whose lengthscale is about 40 mm, as described in the following section.

2.3. *Experimental conditions and characteristic scales*

The wire was heated at two different heating rates. The heat released from the line heat source is partly lost to the surroundings by radiation from the wire and by heat conduction through the Duralumin junctions. Considering such heat losses, the effective heating rates were estimated to be about 267 W/m and 537 W/m (hereinafter, referred to as low heating and high heating, respectively).

For these cases, the ratios of vertical buoyant velocity to the convective velocity were approximately 3×10^{-3} and 4×10^{-3} under low and high heatings, respectively. These values indicate that the buoyancy effect on the thermal evolution process downstream is negligible as has been assumed in most previous experiments for thermal evolution in a turbulent boundary layer.

Mean velocity distributions across the test section at the wire location with and without the heating wire are shown in figure 2. The solid line represents the mean velocity profiles in the wind tunnel without the line heat source. The velocity distribution without the heating wire exhibits a very good uniform shear field. The portion of the uniform shear in the measuring section is about 70% of the test-section height. The upper 20% and the lower 10% of the test section are wall boundary-layer regions. Since the wire diameter is not small enough, there is an appreciable mean velocity wake behind the line heat source as can be seen in figure 2. It was found that such velocity wake patterns virtually disappear at a downstream distance equivalent to a convective lengthscale L_x from the source. This will be mentioned below.

Since the timescale of the large eddy motion in the wind tunnel is imposed by the mean strain rate S of 3.38 s^{-1}, the imposed timescale $\mathscr{T}_{im}$ is 0.296 s. An imposed convective lengthscale is then determined by a relation $L_x = U_c \mathscr{T}_{im}$ where U_c is the centreline mean velocity of 7.85 m/s, hence, $L_x = 2.32$ m. The integral timescale at the source position, $\mathscr{T}_0$, is estimated to be about 5.92 ms by integrating the autocorrelation curve up to the zero-crossing. The integral lengthscale is then $l_0 = U_c \mathscr{T}_0 = 4.65$ cm. Usually, the mean and r.m.s. temperature profiles are scaled by the peak temperature T_p of the mean temperature profile at the downstream station and the vertical distance y is scaled by the half-width of the mean temperature profile L_b. Accordingly, in the following sections, unless otherwise specified, the vertical distance is normalized by L_b, the downstream distance by L_x, the mean and r.m.s. temperature by T_p and the quantity of time dimension is scaled by the imposed timescale $\mathscr{T}_{im}$.

Before presenting our results, it may be necessary to discuss the effect of vortex shedding on the temperature field due to the existence of the wire of finite size.

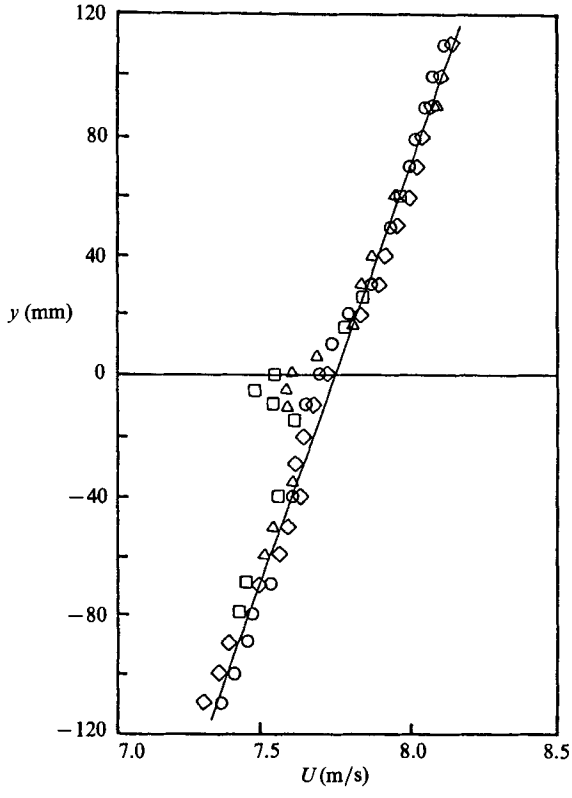

FIGURE 2. Streamwise mean velocity distributions in the range of measurements with and without the heat source. Symbols are mean velocity data with the heating wire: □, $x = 320$ mm; △, $x = 720$ mm; ○, $x = 1320$ mm; ◇, $x = 1910$ mm. The straight line represents the mean velocity profile at the source position without the wire.

Among previous similar experiments of thermal dispersion from a line heat source, the unheated wire Reynolds number of Raupach & Legg (1983) was 450, those of Warhaft (1984) were 38, 175 and 280 and Stapountzis *et al.* (1986) performed their experiments for $Re = 42$ and 207. The latter has additionally studied the effect of the vortex shedding on the thermal evolution. They found that the vortex street after a thicker wire ($d_w = 0.7$ mm) produces a lower peak mean temperature and higher r.m.s. temperature fluctuations in the range of $x/M < 1$ or $x < 30\,d_w$, where d_w is the wire diameter.

Still further downstream, however, both distributions were found to be indistinguishable compared to those from a thinner wire. Warhaft (1984) also checked the dependence of the evolution of θ' on the wire diameter with three different wires whose unheated Reynolds number varied from 39 to 280. The result showed that there was virtually no difference in the mean temperature and r.m.s. temperature profiles in $x/M > 8$. Such experimental evidences are supported by a recent analysis of Sawford and Hunt (1986), who showed that the source size dependence occurs only when the wire diameter is much larger than the Kolmogorov's lengthscale ($d_w \gg \eta$).

During our preliminary experiment with $Re = 380$, it was found that wavy velocity signals at about 2 kHz ($= 0.2\,U_c/d_w$) which is the vortex shedding frequency

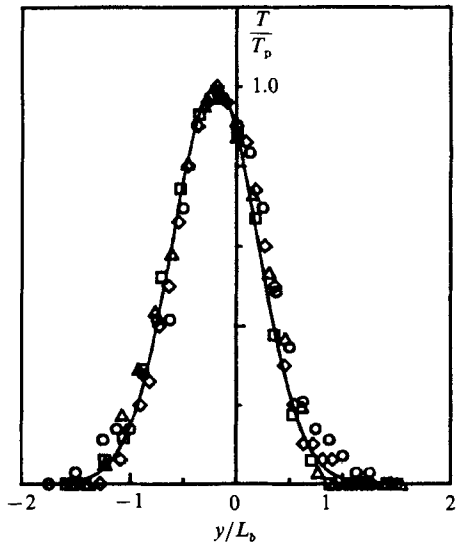

FIGURE 3. Vertical distributions of mean temperature at various downstream positions. Symbols as in figure 2.

(Stapountizis *et al.* 1986) completely disappeared at 100 mm (or $125d_w$) downstream from the wire.

The Kolmogorov's microscale in our uniform shear flow was about 0.6 mm, thus $d_w \sim \eta$. Considering all these facts, it may be concluded that the thermal field in the measurement range of this experiment $x/M > 9$, where M is roughly equivalent to the channel width of the shear generator, was not influenced by the vortex shedding.

The extent of the influence of the uniform shear on the turbulence structure at a point of measurement is represented by the dimensionless flow development time $\tau \equiv (x/U_c)(\mathrm{d}U/\mathrm{d}y)$. In previous velocity field measurements in the homogeneous shear flow in a wind tunnel, the values were 3.6 (Champagne, Harris & Corrsin 1970), 13 (Harris, Graham & Corrsin 1977) and up to 25 (Rohr *et al.* 1988). In our preliminary experiments, it was found that if the strain rate is large, the range of the homogeneous shear field across the flowing area diminishes. Since the thermal field evolves laterally, our measurements were limited up to $x = 1910$ mm downstream from the heat source under the present strain rate in order to guarantee the thermal dispersion well within the homogeneous shear field. This point corresponds to $\tau = 0.82$ which is very low compared to $\tau = 4$, a lower limit for the given shear rate to affect the turbulence field (Rohr *et al.* 1988). Therefore, the effects of shear are not likely to be dominating in the present measurements.

3. Results and discussions

3.1. *Mean temperature and r.m.s. temperature profiles*

The mean temperature profiles normalized by the temperature half-width L_b and the peak temperature T_p of the profile are shown in figure 3.

As can be seen in this figure, the profiles are not Gaussian and their centres shift gradually downward along the downstream distance. Scaling the y distance by the temperature half-widths L_b makes the centre positions of the profiles coincide with

	X/L_x			
	0.155	0.310	0.569	0.823
Peak temperature T_p(°C)	1.72/3.58	1.03/2.05	0.72/1.35	0.50/1.10
Half width, L_b(mm)	17.0/16.0	26.5/27.5	41.0/42.5	54.2/56.0
Downward shift, δ_p(mm)	−4.5/−4.0	−6.0/−5.5	−7.7/−7.5	−10.0/−9.5
Mean displacement, $\bar{y}$(mm)	−4.05/−3.69	−5.75/−4.92	−7.42/−6.73	−8.66/−8.15
Mean dispersion (mm)	5.72/7.22	10.3/12.0	16.2/17.9	20.4/24.6
Skewness	−0.132/−0.018	−0.185/0.049	−0.025/0.035	0.084/0.064
Flatness	2.78/2.91	2.93/2.88	2.81/2.71	2.79/2.82
Lagrangian scalings				
Distance, X/L_L	0.466/0.358	0.931/0.719	1.71/1.31	2.47/1.90
Peak temperature, T_p/θ_L	0.614/0.834	0.368/0.477	0.257/0.315	0.179/0.256
Dispersion, $\langle(y-\bar{y})^2\rangle^{\frac{1}{2}}/l_L$	0.572/0.554	1.03/0.921	1.62/1.37	2.04/1.89

TABLE 1. Evolution characteristics of mean temperature field (low heating/high heating)

each other. The mean temperature profiles $T_{(y)}$ can be statistically characterized by the various centroid-centred moments

$$\langle(y-\bar{y})^n\rangle = \int_0^\infty (y-\bar{y})^n T_{(y)}\,dy \Big/ \int_0^\infty T_{(y)}\,dy,$$

where $\bar{y}$ is the first moment of the mean temperature profile

$$\bar{y} = \int_0^\infty y T_{(y)}\,dy \Big/ \int_0^\infty T_{(y)}\,dy.$$

Since $T_{(y)}$ is approximately equal to the probability that a particle from the source can be found at the point (x, y) (Shlien & Corrsin 1976), the first moment $\bar{y}$ is approximately equal to the mean particle displacment normal to the mean flow direction, and the second centroid-centred moment is equal to the mean vertical dispersion of the particles.

Properties of the mean temperature profiles at various downstream positions under two heating rates are tabulated in table 1. Comparing the downward shift of the peak temperature, δ_p, and computed mean displacement $\bar{y}$ in figure 4, it can be seen that the mean displacement $\bar{y}$ is smaller in magnitude by about 8%, but the trend is almost the same as the downward shift of the peak temperature δ_p. The temperature half-width L_b increases almost linearly with the downstream distance but the mean dispersion $\langle(y-\bar{y})^2\rangle^{\frac{1}{2}}$ is proportional to the square root of the distance from a virtual origin of the heat source; i.e. $D^2 \sim (x-x_0)$. For high heating, the dispersion is larger and the mean downward displacement is smaller than for low heating, as was expected. The skewnesses of the mean temperature profiles in figure 3 are tabulated in table 1. The skewness first has a negative value and then changes sign to a certain positive value downstream. It changes to positive values earlier for high heating than for low heating. This may be attributable to the stronger buoyancy effect of high heating. Shlien & Corrsin (1976) measured a dispersion field from a line heat source in a turbulent boundary layer parallel to, and located at, various vertical distances from the bottom wall. According to their observation, downstream variation of the skewness of the mean temperature profiles for cases when the line heat source was located at $y = 4.16\delta_d$, where δ_d is the displacement boundary-layer

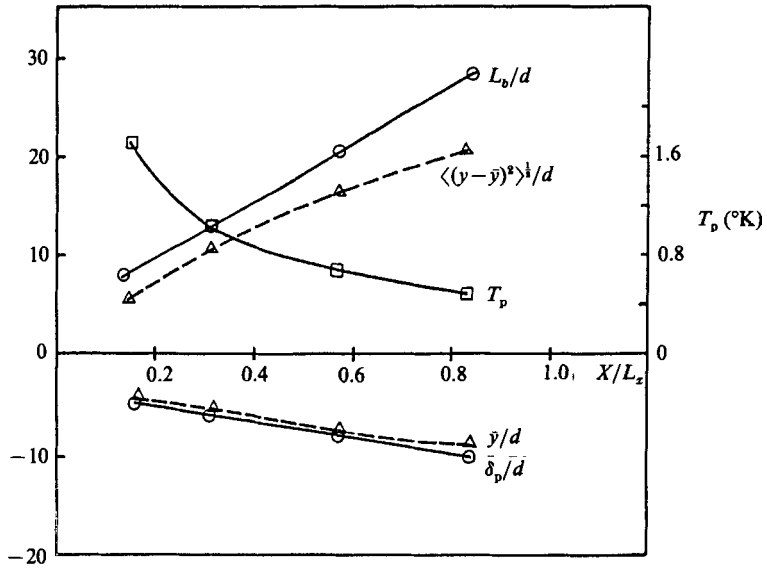

FIGURE 4. Downstream developments of mean temperature half width L_b/d, mean dispersion $\langle(y-\bar{y})^2\rangle^{\frac{1}{2}}/d$, mean displacement $\bar{y}/d$, downward shift of the peak temperature δ_p/d and the decay of peak temperature T_p, where d is the diameter of the heating wire ($d = 0.8$ mm).

thickness, exhibits the same tendency as in the present study. It may be reasoned that, at first, the passive scalar disperses more downward owing to wind shear, but, the thermally stable stratification in the lower part of the thermal wake begins to suppress the downward dispersion in the lower part and the thermally unstable one in the upper part causes more spread in the upper tail of the temperature profile.

The kurtosis (or flatness factor) of the mean temperature profiles are also tabulated in table 1. Although a few numerical values of the kurtosis are not satisfactory, it can be noted that the mean temperature profile is more Gaussian near the source and that the profile tends to be flatter with the downstream distance.

In order to compare the present experimental data with other data on the scalar dispersion from an elevated line heat source in a turbulent boundary layer, Lagrangian scales (Dupont, Kabiri & Paranthoen 1985) are employed to non-dimensionalize the peak temperature T_p and the mean dispersion $\langle(y-\bar{y})^2\rangle^{\frac{1}{2}}$. The Lagrangian temporal integral scale is calculated by the experimental data on the mean dispersion. The results for low and high heatings are tabulated in table 1 with pertinent length and temperature scales. Figure 5 shows the decay of the peak temperature and the downstream evolution of the mean dispersion. Even though the mean velocity field near the source wire in a turbulent boundary layer is not of nearly uniform shear in many experiments cited above, it is noted that our dispersion data correlate well with others in turbulent boundary layers as can be seen in the figure.

The vertical distributions of r.m.s. temperature fluctuations θ' normalized by the peak temperature T_p at various downstream distances are shown in figure 6. The solid line is obtained by fitting a Gaussian profile with the same dispersion as the data. The θ'-distribution has no pronounced double peaks at all X positions over the range of measurement. The appearance of a double peak has been observed and explained by Warhaft (1984) and also theoretically predicted by Stapountzis *et al.* (1986). Both these previous studies show that the double peak disappears at about $x/M \sim 2$ where

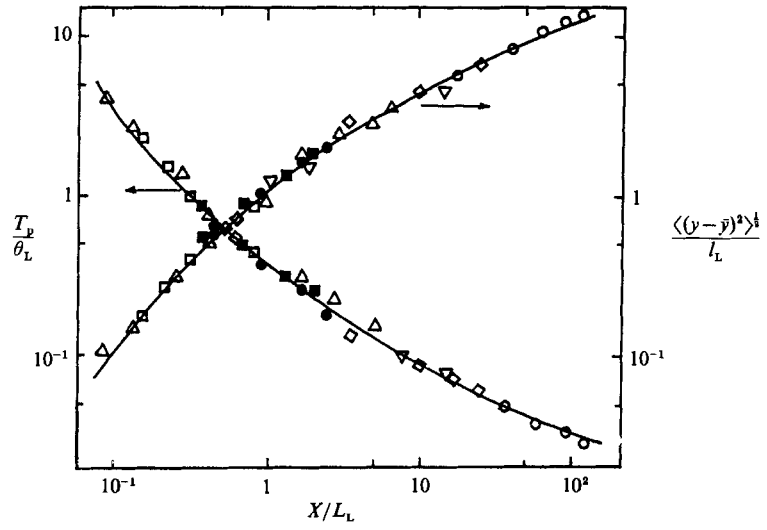

FIGURE 5. Comparisons between the present data and other experiments on the streamwise evolutions of peak temperature and the mean dispersion. Solid symbols are present data: ●, low heating; ■, high heating. Open symbols are other data in turbulent boundary-layer experiments collected by Dupont *et al.* (1985). Solid lines are smooth-curve fits to these data.

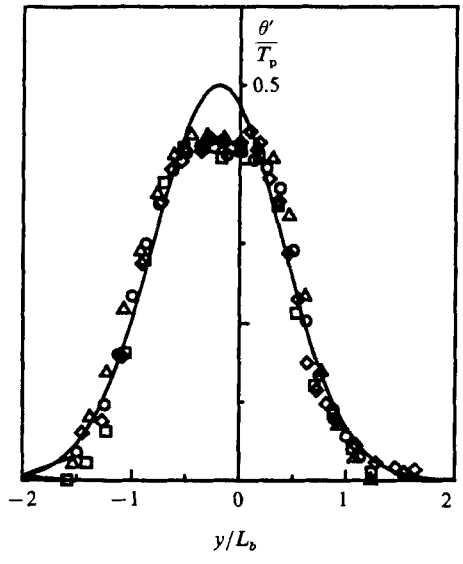

FIGURE 6. Root mean square temperature profiles at various downstream distances. Symbols are as in figure 2. The solid line is a Gaussian curve fit to the data with the same standard deviation as the data.

M is the mesh size of the grid. However, Warhaft (1984) observed re-emergence of the double peak at $x/M = 63$ and 133. Since our integral lengthscale l_0 is approximately equivalent to M, our measurement range is in a range $12 \leqslant x/M \leqslant 41$. Close examination of the original data of figure 6 confirms a tendency for such a double peak to appear again far downstream. The ratio of maximum θ' to the peak temperature T_p in unsheared grid turbulence was reported to be about 0.7 in Warhaft

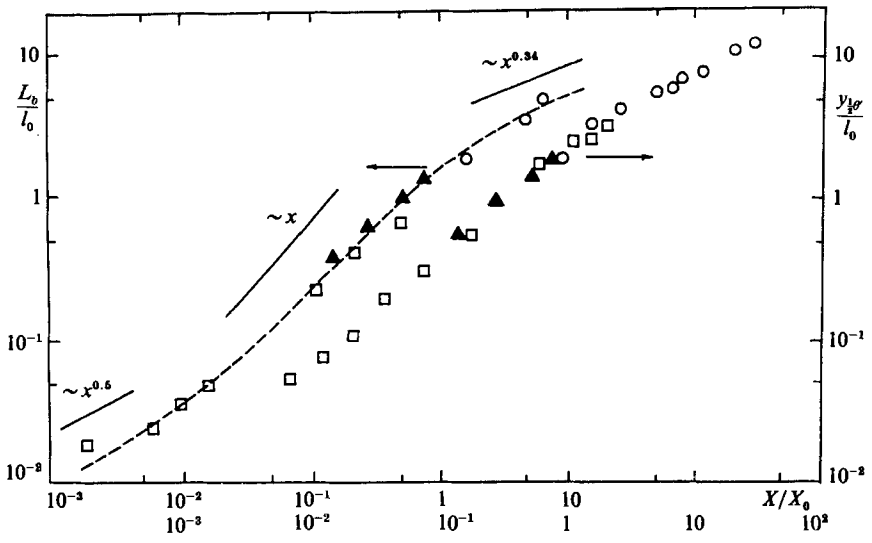

FIGURE 7. Comparisons between present data and data in grid turbulence (Warhaft 1984) on normalized half-widths of the mean temperature profiles (left-hand curve, L_b) and r.m.s. temperature profiles (right-hand curve, $y_{\frac{1}{2}\theta'}$). Solid symbols, present data. Open symbols, Warhaft (1984). The dashed line is the prediction of Anand & Pope (1985).

(1984) and 0.6 in Stapountzis *et al.* (1986), but in our case the ratio is about 0.42. Considering the value of 0.27 obtained by Fabris (1979) who used a thicker cylinder of diameter 6.2 mm, such a difference in the ratio is due to the source wire size; the ratio becomes larger for smaller wire size. The downstream developments of the half-widths of the mean and the r.m.s. θ' profiles are shown in figure 7. Following the proposal of Anand & Pope (1985), the half-widths of the profiles have been normalized by the integral scale l_0 at the location of the heat source and the distances downstream from the source have been normalized by the distance of the source from the screen X_0. The collapse of our data to the curves formed by the data of Warhaft (1984) is remarkable. According to the present data and those of Warhaft (1984), the r.m.s. θ' profile has a wider half-width than that of the mean temperature profile; however, the data of Stapountzis *et al.* (1986) shows the reverse. More experimental observation is necessary to clarify such a discrepancy.

3.2. *Turbulent Reynolds shear stresses and heat fluxes; $\overline{u_i u_j}$ and $\overline{u_j \theta}$*

The r.m.s. values of streamwise and vertical velocity fluctuations u' and v' are normalized by the centreline mean velocity U_c at the source and are shown in figures 8(*a*) and 8(*b*).

Compared with the wake pattern in the mean velocity profile, the wake of the turbulent fluctuations persists comparatively longer owing to the production of the turbulent kinetic energy by an amount $-\overline{uv}\,\mathrm{d}U/\mathrm{d}y$. This is consistent with the observations by Shlien & Corrsin (1976) and Champagne *et al.* (1970). In comparison with the persistence of the wake property of the measurement of Raupach & Legg (1983) in a turbulent boundary layer, the restoration to the free-stream condition is rather slower in the present experiment. In the usual two-dimensional wake behind a cylinder, u'-distribution has two peaks at both sides of the wake even in the self-preservation region (Townsend 1976). In our case, since the two peaks of u'-profile

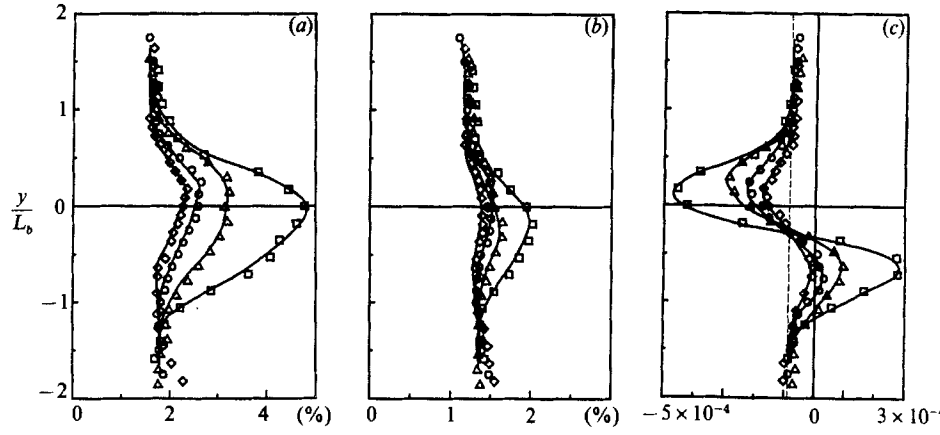

FIGURE 8. Distributions of component intensities and Reynolds shear stresses: (*a*) u'/U_c, (*b*) v'/U_c, (*c*) $\overline{uv}/U_c^2$. Symbols as in figure 2. The dashed line in (*c*) represents the Reynolds shear stress of the free stream (outside of the velocity wake).

formed in the initial stage of evolution are exposed to two differently straining field, i.e. locally high shear in the upper part and locally low shear in the lower part, the bulge of the u'-value in the upper part and the shrinkage in the lower part together make the u'-profile merge into the u'-profile of a single peak. The v'-distribution in figure 8(*b*) has a similar structure to that of the u'-distribution. The profile skews in the lower half and the peak position tends to shift upward. Both the u'- and v'-values at the centreline approach the free-stream values far downstream. Distributions of the mean Reynolds shear stress $\overline{uv}$ are shown in figure 8(*c*). They are similar in shape to the plane wakes and jets (Townsend 1976). It appears that the profile is a superposition of the plane wake onto the homogeneous uniform shear flow with gradual downward shift. It is not clear how to identify the measure of downward shift of the dynamic field. The point of maximum mean velocity defect almost coincides with the point of zero crossing of the $\overline{uv}$-profile. At far downstream, however, the $\overline{uv}$-profile does not cross the zero level. But, it is noted that the points of the free-stream value of $\overline{uv}$ collapse nearly on a single point when the y-distance is scaled by L_b. Therefore, the point at which $\overline{uv}$ has the same value as that of the free stream is considered to be an appropriate measure of the downward deflection of the dynamic field.

Figure 9(*a*) shows the profile of the vertical heat flux $\overline{v\theta}$. The downward deflection of thermal field at each measurement position may be measured by the zero crossing point which is almost coincident with the point of the peak temperature T_p. The $\overline{v\theta}$ profile shape is antisymmetrical with the peak value in the lower part a little smaller. This implies that the vertical heat flux upward is larger than that in the downward direction. The weakness of the mean shear effect on $\overline{v\theta}$ is due to the fact that production term in the $\overline{v\theta}$ equation does not contain the mean shear or the Reynolds shear stress $\overline{uv}$. The overall shape of $\overline{v\theta}$ is very similar to that in a plane heated wake by Fabris (1979); the mean shear has a small effect on the $\overline{v\theta}$ profile only indirectly.

In contrast to the $\overline{v\theta}$-profile, the streamwise heat flux $\overline{u\theta}$ shown in figure 9(*b*) has a strong effect on the mean shear. One of the production terms in the governing equation for $\overline{u\theta}$ is $-\overline{v\theta}\,\mathrm{d}U/\mathrm{d}y$ whose magnitude is of significant size throughout the field of measurement. The higher value in the upper part is due to the larger value of $\overline{v\theta}$ and larger local mean velocity gradient there. Note that $\overline{u\theta}$ has negative sign

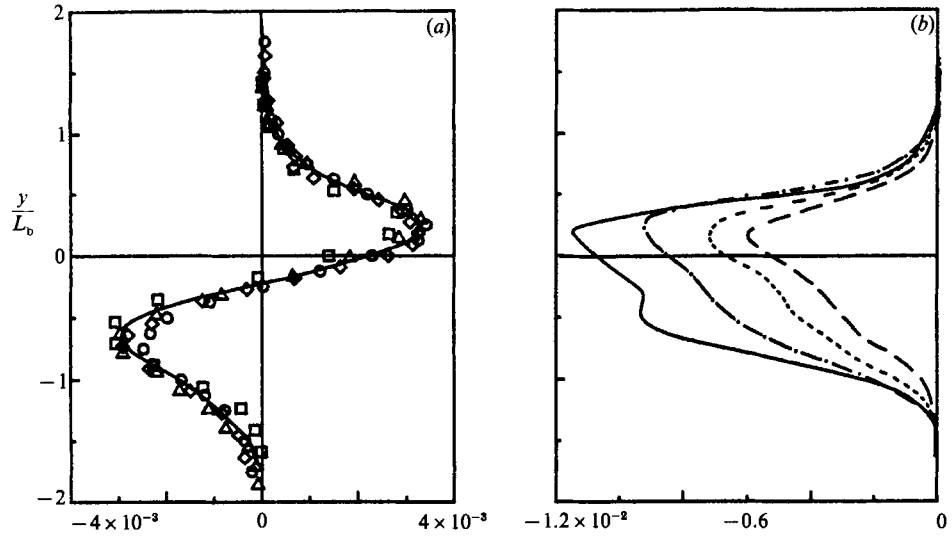

FIGURE 9. Turbulent heat flux distributions. (*a*) $\overline{v\theta}/U_c T_p$. Streamwise heat flux: ——, $x/L_x = 0.155$; —·—, $x/L_x = 0.31$; – – –, $x/L_x = 0.569$; ——, $x/L_x = 0.823$. (*b*) $\overline{u\theta}/U_c T_p$. Vertical heat flux; symbols as in figure 2.

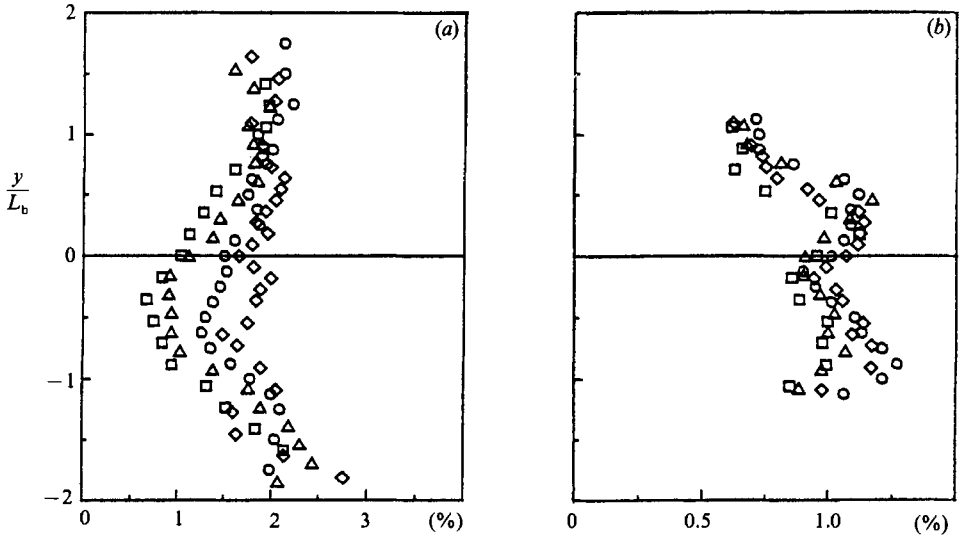

FIGURE 10. Distributions of normalized timescales. (*a*) Velocity timescales, $\mathscr{T}/\mathscr{T}_{im}$, (*b*) temperature timescale, $\mathscr{T}_\theta/\mathscr{T}_{im}$. Symbols as in figure 2.

in the whole field, as in the plane heated wake (Fabris 1979). However, in a dispersion measurement in a turbulent boundary layer (Raupach & Legg 1983), $\overline{u\theta}$ changes sign from negative to positive at the heat source height. The ratio between the vertical heat flux $\overline{v\theta}$ and the horizontal heat flux $\overline{u\theta}$ near the peak positions of $\overline{v\theta}$ is roughly 3, which is consistent with Monin & Yaglom (1971, p. 522).

3.3. *Integral timescales, dissipations and anisotropy*

The integral timescale variation of velocity $\mathscr{T}$ and temperature $\mathscr{T}_\theta$ are depicted in figure 10(*a*, *b*). The timescale was obtained by integrating the auto-correlation curve

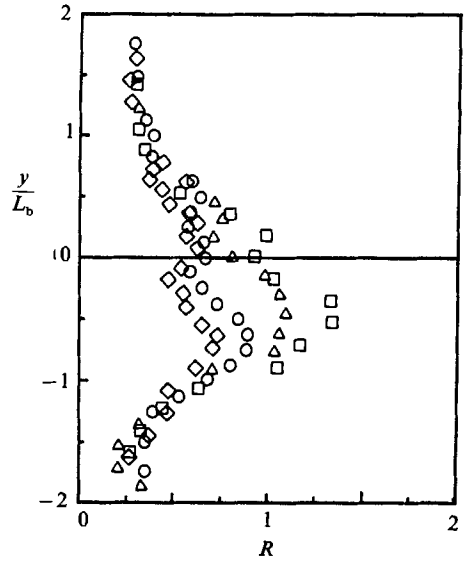

FIGURE 11. Timescale ratios between temperature and velocity, $R = \mathscr{T}_\theta/\mathscr{T}$. Symbols as in figure 2.

up to the zero crossing point (Champagne *et al.* 1970). Owing to the velocity wake, the velocity timescale varies significantly in the range of the experiment, whereas the temperature timescale increases very slowly along the downstream distance. There are double peaks in the $\mathscr{T}_\theta$ profiles which are roughly coincident with the positions of maximum slope of the θ' profile (see figure 6). The integral timescale ratio $R(=\mathscr{T}_\theta/\mathscr{T})$ at the edge of the wake profile is about 0.3 and within the wake region it varies between 0.5 and 1.3 (figure 11). It decreases with the downstream distance with the maximum in the lower part. The higher value in the lower part is attributable to the downward shift of the larger thermal mass.

The rate of kinetic energy dissipation ϵ and the destruction of temperature variance ϵ_θ which are non-dimensionalized by local scales are obtained as in figure 12. The rate of dissipation was evaluated by the following inviscid estimates (Tennekes & Lumley 1972),

$$\epsilon = ((\overline{u^2}+\overline{v^2})/2)^{\frac{3}{2}}/l, \quad l = \mathscr{T}U.$$

Likewise ϵ_θ has been estimated as

$$\epsilon_\theta = \overline{\theta^2}/l_\theta, \quad l_\theta = \mathscr{T}_\theta U.$$

It is seen that both ϵ and ϵ_θ have maximum values in the centre region and that ϵ decreases much faster than ϵ_θ along the downstream distance. Figure 13 shows the decay of anisotropies II and II_θ and the variation of the timescale ratio R along the centreline. The anisotropy II is defined by $\mathrm{II} = b_{ij}b_{ij}$ where $b_{ij} = \overline{u_iu_j}/\overline{q^2} - 1/3\delta_{ij}$. The scalar flux anisotropy II_θ is defined by $\mathrm{II}_\theta = f_if_i$ where $f_i = \overline{u_i\theta}/(q^2\overline{\theta^2})^{\frac{1}{2}}$ and $\overline{q^2} = \overline{u_iu_i}$. It is shown that the anisotropies II and II_θ both relax to the isotropic state at almost the same rate. The timescale ratio R approaches about 0.5 at far downstream.

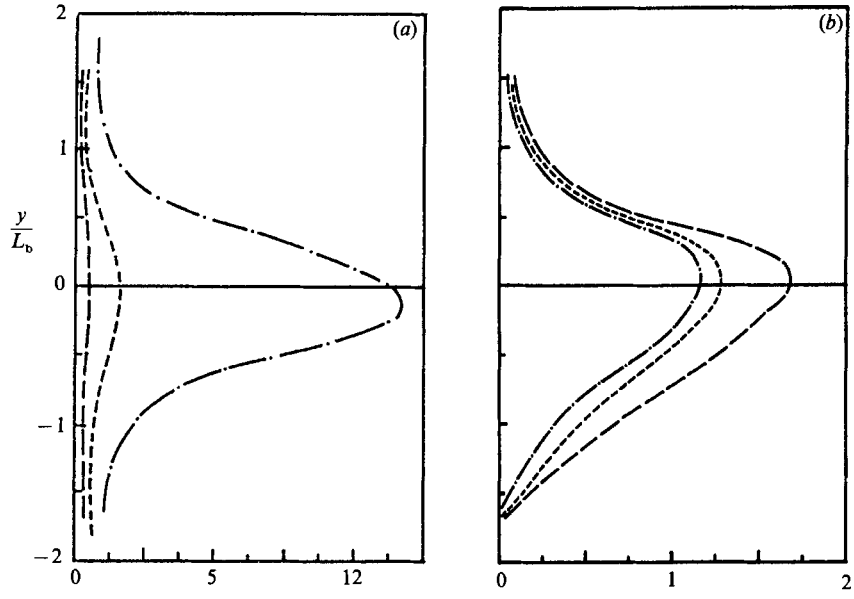

FIGURE 12. Variations of isotropic dissipation profiles and the destruction rate of temperature variance. (*a*) $\epsilon/(L_b^2 \mathscr{T}_{im}^{-3})$, rate of isotropic dissipation, (*b*) $\epsilon_\theta/(T_p^2 \mathscr{T}_{im}^{-1})$, destruction rate of temperature variance. Lines as in figure 9.

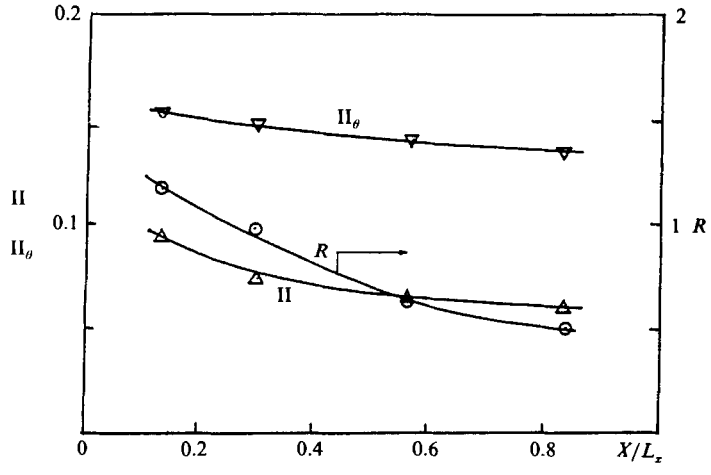

FIGURE 13. Downstream variations of anisotropies II and II_θ and the timescale ratio.

3.4. *Third-order scalar transport terms*

Modelling the turbulent third-order scalar transport terms in dynamic equations of second-order moments such as kinematic heat fluxes $\overline{v\theta}$ and $\overline{u\theta}$, Reynolds stress $\overline{uv}$ and temperature variance $\overline{\theta^2}$ are of fundamental importance in predicting many engineering and geophysical dispersions of heat, moisture or pollutants. The purpose in this section is to test three different models for representing the spatial transports of $\overline{uv}$, $\overline{u\theta}$, $\overline{v\theta}$ and $\overline{\theta^2}$ in non-isothermal turbulent flows with the present measurements.

One of the simplest ones is the simple gradient transport model. Specifically, for boundary-layer flows, they are as follows (Launder 1978):

$$\overline{uv^2} = -\tau_3\left(2\overline{v^2}\frac{\partial\overline{uv}}{\partial y}+\overline{uv}\frac{\partial\overline{v^2}}{\partial y}\right),$$

$$\overline{uv\theta} = -\tau_3\left(\overline{uv}\frac{\partial\overline{v\theta}}{\partial y}+\overline{v^2}\frac{\partial\overline{u\theta}}{\partial y}\right),$$

$$\overline{v^2\theta} = -2\tau_3\overline{v^2}\frac{\partial\overline{v\theta}}{\partial y},$$

$$\overline{v\theta^2} = -\tau_3\overline{v^2}\frac{\partial\overline{\theta^2}}{\partial y},$$

where τ_3 is an appropriate timescale for the third-order moments. It has often been asserted that the timescale τ_3 may be substituted by the dynamic timescale $\tau_u(=\overline{q^2}/\epsilon)$. Conventionally, the following form has been used,

$$\tau_3 = 0.055\,\overline{q^2}/\epsilon.$$

This is possible only if one assumes that the thermal timescale $\tau_\theta(=\overline{\theta^2}/\epsilon_\theta)$ is almost proportional to τ_u. However, since the timescale ratio R has been proved to vary in the range of $0.3 < R < 1.3$, such an assumption is not adequate. Recently, Chung & Kyong (1986) have proposed a composite timescale in the form of a simple weighted algebraic mean between τ_u and τ_θ to be used for τ_3 in conjunction with the simple gradient transport model in the following form,

$$\tau_3 = 0.055\,\tau_u(1+b\tau_\theta/\tau_u).$$

The constant b is assumed to depend on the power of temperature fluctuations θ in the moments: namely, $b = 0$ for $\overline{u^2v}$, $\overline{uv^2}$ and $\overline{v^3}$, $b = 1$ for $\overline{uv\theta}$ and $\overline{v^2\theta}$, and $b = 2$ for $\overline{v\theta^2}$. This model reflects the fact that a larger contribution comes from the thermal timescale for higher powers of fluctuating temperature θ in the triple moments.

For a horizontally homogeneous atmospheric boundary layer under buoyancy effects, Zeman & Lumley (1979) explicitly expressed the third-order moments in terms of various turbulence timescales, the Brunt–Väisälä frequency and gradients of the second-order quantities in a tensorial form. This model has been tested in Chung & Kyong (1986) and it was found that the model overpredicts most third-order moments. Under further assumptions of weak inhomogeneity in temperature and negligible buoyancy effect, Lumley (1978) has presented a closed set of linear equations for $\overline{u_i\theta^2}$, $\overline{u_iu_j\theta}$ and $\overline{u_iu_ju_k}$ as follows:

$$\overline{\theta^2}_{,k}\,\overline{u_ju_k}+2(\overline{u_j\theta})_{,k}\,\overline{u_k\theta} = -2(\bar{\epsilon}_\theta/\overline{\theta^2})\,[1+C_\theta(\bar{\epsilon}/\bar{q}^2)\,(\overline{\theta^2}/\bar{\epsilon}_\theta)]\,\overline{u_j\theta^2},$$

$$\begin{aligned}&(\overline{u_i\theta})_{,k}\,\overline{u_ku_j}+(\overline{u_j\theta})_{,k}\,\overline{u_ku_i}+(\overline{u_iu_j})_{,k}\,\overline{\theta u_k}\\&\quad = -[C_1(\bar{\epsilon}/\bar{q}^2)\,(\overline{u_iu_j\theta}-\overline{q^2\theta}\,\delta_{ij}/3)+(2\bar{\epsilon}/3\bar{q}^2)\,\overline{q^2\theta}\,\delta_{ij}+2C_\theta(\bar{\epsilon}/\bar{q}^2)\,\overline{u_iu_j\theta}],\end{aligned}$$

$$\begin{aligned}&(\overline{u_iu_j})_{,p}\,\overline{u_ku_p}+(\overline{u_iu_k})_{,p}\,\overline{u_iu_p}+(\overline{u_ju_k})_{,p}\,\overline{u_iu_p}\\&\quad = -3C_1(\bar{\epsilon}/\bar{q}^2)\,[\overline{u_iu_ju_k}-(\tfrac{1}{9})\,(\delta_{ij}\overline{q^2u_k}+\delta_{ik}\overline{q^2u_j}+\delta_{ij}\overline{q^2u_i})]\\&\qquad -(2\bar{\epsilon}/3\bar{q}^2)\,(\delta_{ij}\overline{q^2u_k}+\delta_{ik}\overline{q^2u_j}+\delta_{jk}\overline{q^2u_i}).\end{aligned}$$

In the following discussions, model predictions by the above simple gradient transport model with the dynamic timescale for τ_3, and that with our new composite

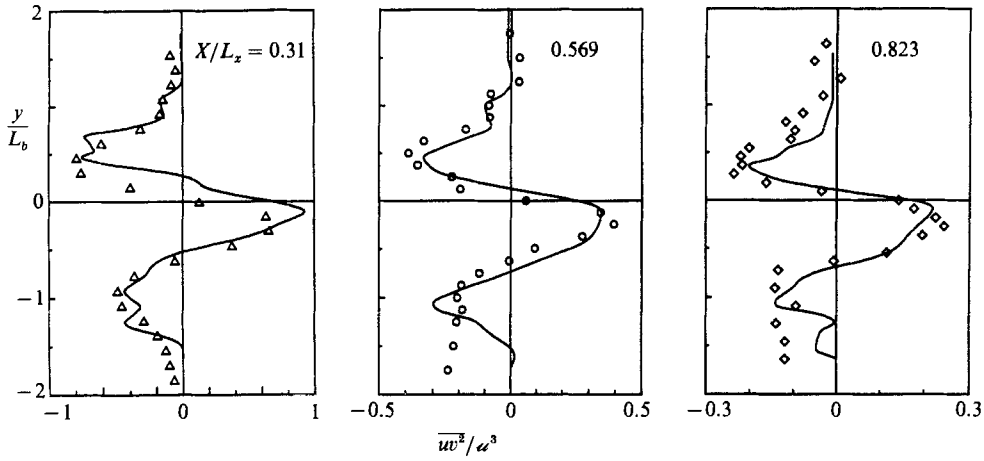

FIGURE 14. Comparison of model predictions with data of $\overline{uv^2}/\mathscr{u}^3$ where $\mathscr{u}^2 = \frac{1}{3}\overline{u_i u_i}$ at various downstream distances. Prediction: ——, present composite timescale model. Symbols as in figure 2.

timescale for τ_3 and Lumley's model are compared, together with the present experimental data. All predictions are computed with the directly measured values. In the following figures, symbols represent our data, the solid line is the predicted profile by our composite timescale model, the dotted line by Lumley's (1978) model and the dashed line by the conventional simple gradient transport model.

Figure 14 shows the comparison of predictions with the data of $\overline{uv}^2$, the streamwise transport of $\overline{v}^2$ or vertical transport of $\overline{uv}$. (Here, Lumley's model was not tested owing to lack of data on transverse velocity fluctuations w.) The gradient of $\overline{uv}^2$ appears as a turbulent diffusion term in the governing equation of Reynolds stress. Note that the zero-crossing point of the $\overline{uv}$-profile nearly coincides with the plus peak positions of the $\overline{uv}^2$-profiles, which means that the turbulent diffusion of $\overline{uv}$ is negligible at the zero-crossing point. The profile is similar to that of a heated plane wake of Fabris (1983). The vertical position of the positive peak in the lower part nearly coincides with the maximum velocity wake also. This is in contrast with the heated plane jet where $\overline{uv}^2$ is negative in the central part and becomes positive in the outer free mixing zone (Dekeyser & Launder 1985). The simple gradient transport model predicts $\overline{uv}^2$ fairly well. The abnormal variations of the predicted profiles at both peaks at $x/L_x = 0.32$ are due to scatter of experimental data of second-order moments.

Figure 15 shows the profile of $\overline{uv\theta}$, the streamwise transport of $\overline{v\theta}$. The profile is similar to that in the dispersion measurement from a line heat source in a turbulent boundary layer (Raupach & Legg 1983) except near the wall layer. In the heated plane wake of Fabris (1983), $\overline{uv\theta}$ vanishes at the wake centre and changes sign from positive to negative along the outward direction. In our case and in the turbulent boundary layer, $\overline{uv\theta}$ does not vanish at the thermal jet centre. Predictions are fairly reasonable except for the simple gradient model which underpredicts $\overline{uv\theta}$ in the whole region by a factor of about 2.

Figure 16 represents the streamwise transport of $\overline{u\theta}$, i.e. $\overline{u^2\theta}$-profiles. The profiles are everywhere positive in the upper and lower parts, which is different from the heated jet (Dekeyser & Launder 1985) where it has smaller negative value in the central region. It is noted that predictions by the present model are of the same magnitude as those by Lumley's model. All model predictions are low compared with

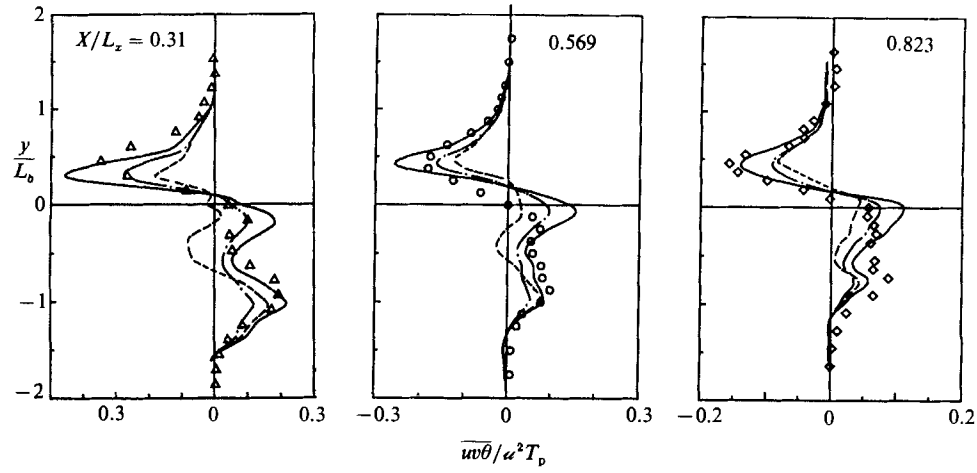

FIGURE 15. Comparison of model predictions with data of $\overline{uv\theta}/u^2T_p$. Predictions: ——, present composite timescale model; —·—, simple gradient model; – – –, Lumley's (1978) linear algebraic equation model. Symbols as in figure 9.

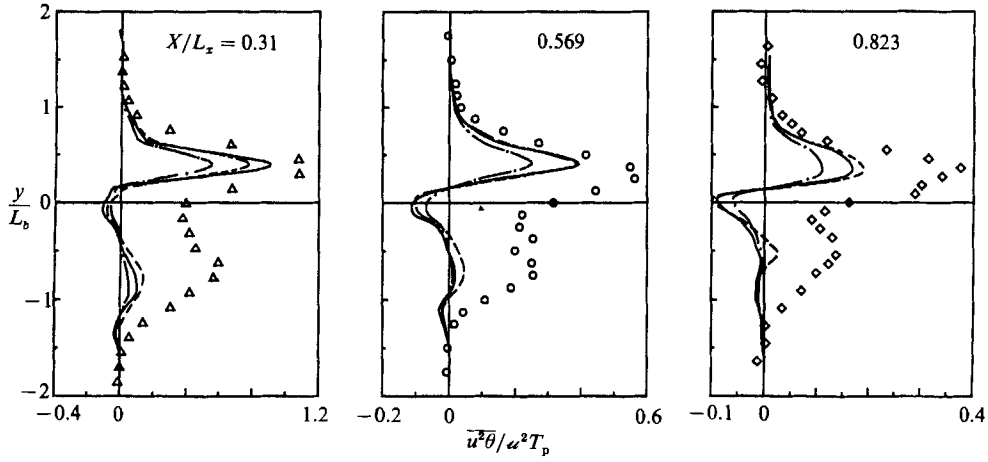

FIGURE 16. Comparison of model predictions with data of $\overline{u^2\theta}/u^2T_p$. Lines and symbols as in figure 15.

the data, which may imply that the timescale for the streamwise transport should be different from that for vertical transport.

The vertical transport of the vertical heat flux, $\overline{v^2\theta}$, is represented in figure 17 (a, b) for low heating and for high heating, respectively. The vertical gradient of $\overline{v^2\theta}$ is the turbulent diffusion term in the boundary-layer-type governing equation of $\overline{v\theta}$. Two zero crossings are located near the peaks of $\overline{v\theta}$ and the negative peaks coincide with the zero crossings of $\overline{v\theta}$. This means that the diffusion of $\overline{v\theta}$ by turbulent vertical fluctuations is strongest at the peaks of $\overline{v\theta}$ since the maximum slopes of $\overline{v^2\theta}$ are near these points, and the diffusion of $\overline{v\theta}$ by vertical fluctuations is negligible at the zero crossing of $\overline{v\theta}$. The profiles are similar to the heated plane wake but with downward shift of the profile. The same trend can also be seen in Raupach & Legg (1983) and Dekeyser & Launder (1985). The predictions by the simple gradient-transport model

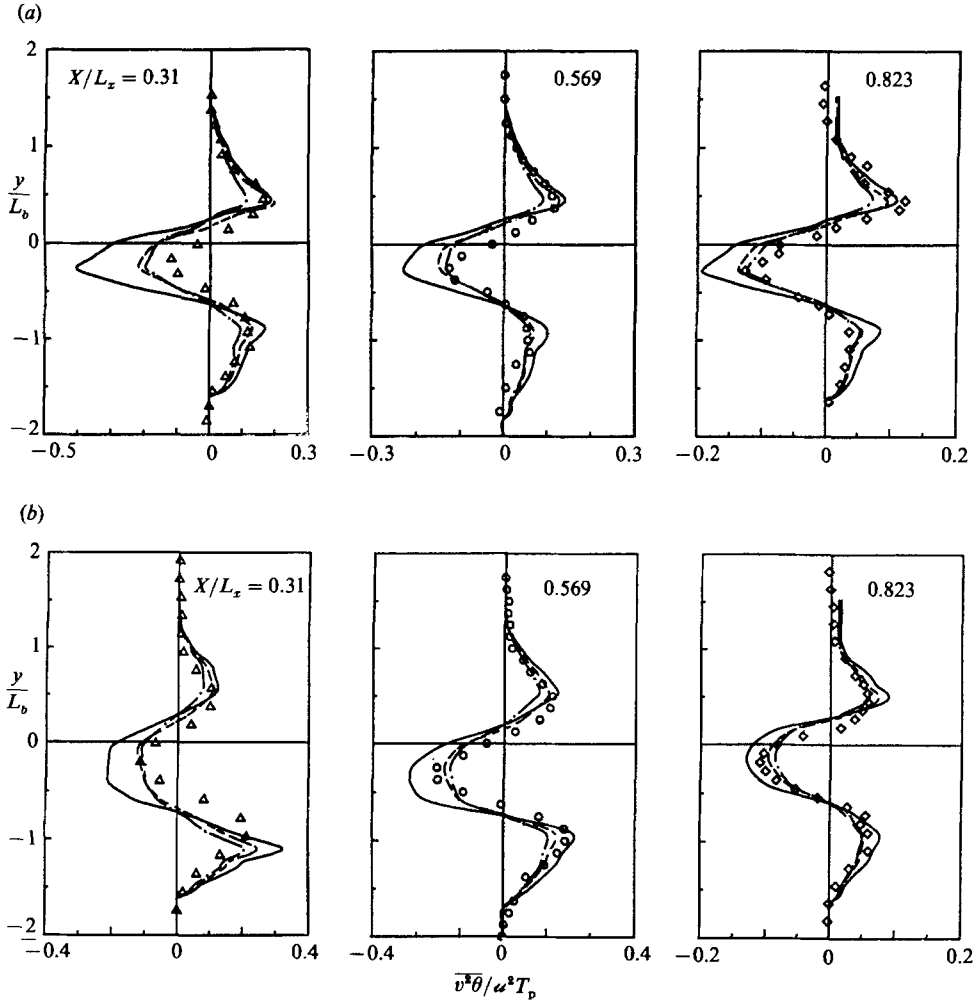

FIGURE 17. Comparisons of model predictions with data of $\overline{v^2\theta}/u^2T_p$; (*a*) low heating, (*b*) high heating. Lines and symbols as in figure 15.

and Lumley's model are fairly good, but our model overpredicts the negative peak region of the profile. Such over-predictions are not serious in the case of high heating as can be seen in figure 17(*b*).

In figure 18 profiles of $\overline{u\theta^2}$, the streamwise transport of $\bar{\theta}^2$, are presented. $\overline{u\theta^2}$ remains negative in the whole region with two peaks on both sides. In the heated plane wake of Fabris (1983), the $\overline{u\theta^2}$ which is slightly positive near the centre becomes highly negative in the outer free mixing region. But, in the heated plane jet of Dekeyser & Launder (1985), the $\overline{u\theta^2}$-profile is highly negative in all the upper part of the jet but with some peak positive value in a narrow region of the lower part. Only Lumley's model predicts the $\overline{u\theta^2}$ level reasonably in the upper field, but, the simple gradient model under-predicts $\overline{u\theta^2}$ in the whole field. This again may imply that the streamwise transport of $\bar{\theta}^2$ must have a different timescale from other vertical transports.

Finally figure 19(*a*) and 19(*b*) show the profiles of $\overline{v\theta^2}$, the vertical transport of the temperature variance for low heating and high heating, respectively. It is noted that

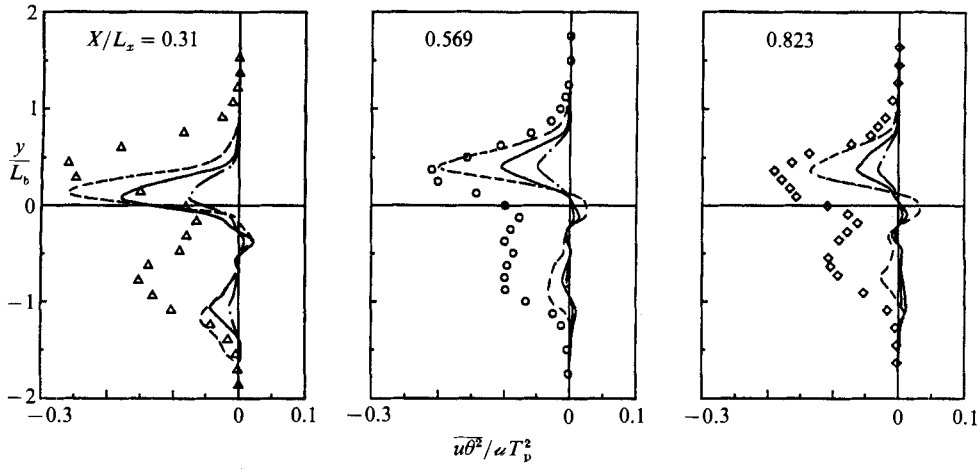

FIGURE 18. Comparison of model predictions with data of $\overline{u\theta^2}/uT_p^2$. Lines and symbols as in figure 15.

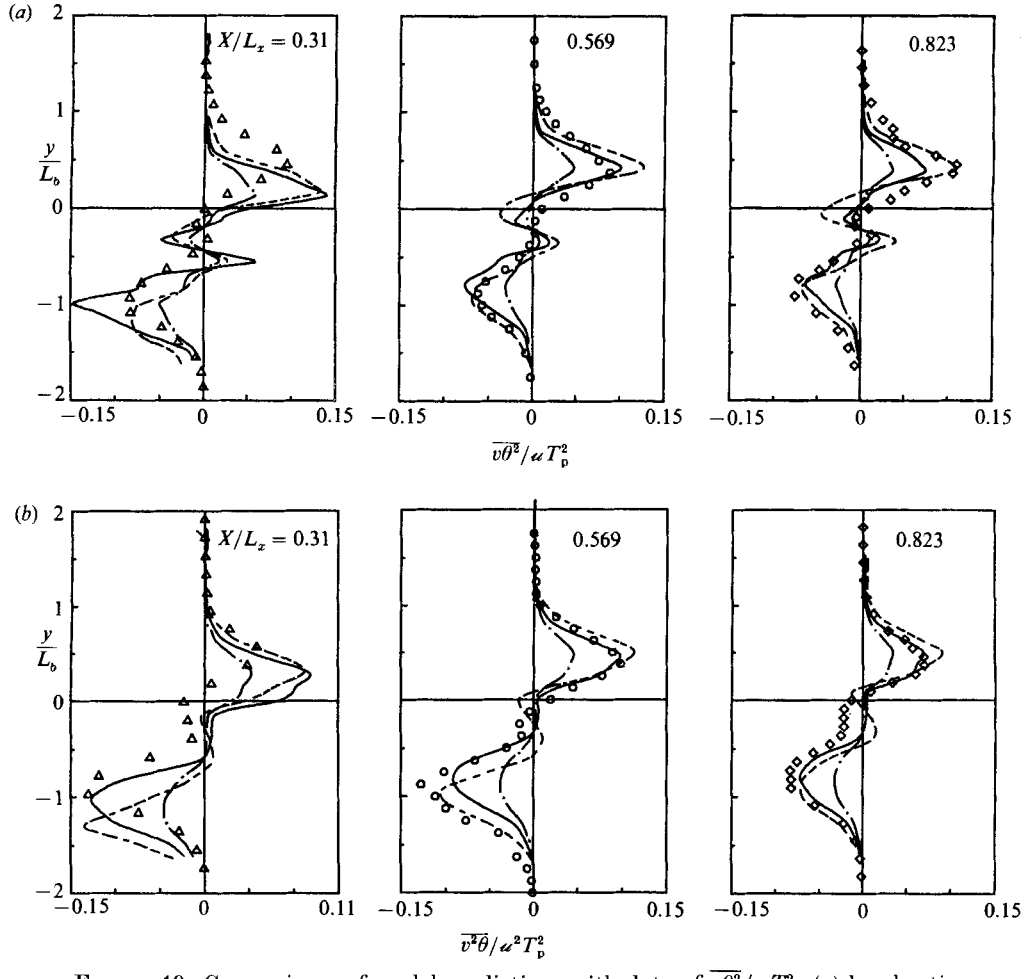

FIGURE 19. Comparisons of model predictions with data of $\overline{v\theta^2}/uT_p^2$; (*a*) low heating, (*b*) high heating. Lines and symbols as in figure 15.

the profiles are nearly anti-symmetric with respect to the centre position of the $\overline{\theta^2}$ profiles. The peak values in the centre region are much smaller than those in the outer edge regions, which is consistent with Fabris' (1983) data of $\overline{v\theta^2}$ in the plane heated wake and with Raupach & Legg's (1983) in a turbulent boundary layer. In the high heating case of figure 19(*b*) the profiles are nearly flat in the centre region. Model predictions by the present composite timescale model are of the same degree of accuracy as those by Lumley's model, whereas, the conventional simple gradient transport model yields under-predictions by about 50% in all cases.

Considering the overall performance of the three models for all the triple moments in this section, it may be concluded that our model, which employs a composite timescale for the simple gradient transport model, yields the best overall predictions with no additional cost.

4. Conclusions

The paper has presented an experimental investigation on the turbulent dispersion of passive temperature behind a fine cylindrical heat source in a homogeneous uniform shear flow. The purpose of presenting this work is mainly to provide valuable basic data for assessment of the currently available third-order transport models. However, since the experiment has its own merit in that the effect of the uniform mean shear on the dispersion of the passive scalar can be investigated by analysing the data presented herein, the data of scalar dispersion field and various second-order moments have been analysed at some length in the first part of the paper. It was found that the vertical profiles of the mean temperature and the r.m.s. temperature both exhibit nearly Gaussian distributions except for a little degradation in the centre region of the r.m.s. temperature profile. The mean temperature data at different downstream distances can well be collapsed onto a simple Gaussian curve with reasonable scatter when they are normalized by the local peak mean temperature and the local temperature half-width. The same argument can be made for the data of r.m.s. temperature profiles.

When the peak temperature, the mean dispersion of the temperature field and the downstream distance are normalized by respective Lagrangian scales proposed by Dupont *et al.* (1985), the peak temperatures and the mean dispersions are well correlated with other data in turbulent boundary layers reported by various authors. A problem, however, in utilizing such Lagrangian scaling is that the Lagrangian integral timescale must be computed from experimental data of the mean scalar dispersion $\langle (y-\bar{y})^2 \rangle$ which can not be known *a priori*.

When the evolution of the scalar field is analysed, Anand & Pope's scalings were used. The downstream distance was normalized by the distance between the screen and the line heat source and the half-widths were normalized by the streamwise integral lengthscale at the source. Such scaling also permitted nice collapse of the present data of the growth of the half-widths onto a single line obtained by the data of Warhaft (1984) and Staupontzis *et al.* (1986). Present data on various second-order moments have been investigated compared to the data in a plane heated wake, plane heated jet and a turbulent boundary layer.

Profiles for statistical moments of velocity fluctuations and rate of dissipation change appreciably with the downstream distance owing to the presence of the wake structure. However, the thermal statistics change slowly with the downstream distance. It has been noted that the streamwise heat flux $\overline{v\theta}$ normalized by local scales remain the same with the downstream distance. The timescale ratio between

temperature and velocity fluctuations varies between 0.3 and 1.3 across the stream and it asymptotes to a value of 0.5 at far downstream.

Finally, data of the third-order velocity–temperature correlations were analysed by three different second-order models; namely, a simple gradient transport model with a conventional dynamic timescale, and that with a simple composite timescale between dynamic and thermal timescales and an extensive mathematical model by Lumley (1978).

As a result of the model predictions, it was found that all models considered here provide the correct trend for the profiles, but, with different levels of accuracy. The simple gradient-transport model with a composite timescale proposed by Chung & Kyong (1986) yields remarkably good numerical values in comparison to a more extensive theoretical model which requires long computational time and cost. An important observation is that all the streamwise transports of second-order moments are badly under-predicted compared to the vertical transports of the same moments. This suggests that the streamwise transport must have timescales different from those for the vertical or cross-stream transport of the second-order moments. It is believed that a comparative study of the present data with previous experiments on thermal turbulence in a grid-generated isotropic turbulence reviewed in §1 should reveal conclusive information on the role of the straining effect on the temperature field.

This research was supported by the Korea Science and Engineering Foundation under Grant No. 812-09-013-2.

REFERENCES

ANAND, M. S. & POPE, S. B. 1985 Diffusion behind a line source in grid turbulence. In *Turbulent Shear Flows 4* (ed. L. J. S. Bradbury, F. Durst, B. E. Launder, F. W. Schmidt & J. H. Whitelaw), pp. 46–61. Springer.

ANTONIA, R. A., BROWNE, L. W. B. & CHAMBERS, A. J. 1981 Determination of time constants of cold wire. *Rev. Sci. Instrum.* **52**, 1382–1385.

BUDWIG, R., TAVOULARIS, S. & CORRSIN, S. 1985 Temperature fluctuations and heat flux in grid-generated isotropic turbulence with streamwise and transverse mean-temperature gradients. *J. Fluid Mech.* **153**, 441–460.

CHAMPAGNE, F. H., HARRIS, V. G. & CORRSIN, S. 1970 Experiments on nearly homogeneous turbulent shear flow. *J. Fluid Mech.* **41**, 81–141.

CHUNG, M. K. & KYONG, N. H. 1986 A simple composite time scale model for third-order scalar transports. *Phys. Fluids* **29**, 3914–3916.

DEKEYSER, I. & LAUNDER, B. E. 1985 A comparison of triple-moment temperature–velocity correlations in the asymmetric heated jet with alternative closure models. In *Turbulent Shear Flow 4* (ed. L. J. S. Bradbury, F. Durst, B. E. Launder, F. W. Schmidt & J. H. Whitelaw), pp. 102–117. Springer.

DUPONT, A., KABIRI, M. EL & PARANTHOEN, P. 1985 Dispersion from elevated line source in a turbulent boundary layer. *Intl J. Heat Mass Transfer* **28**, 892–894.

FABRIS, G. 1979 Conditional sampling study of turbulent wake of a cylinder. *J. Fluid Mech.* **94**, 673–709.

FABRIS, G. 1983 Third-order conditional transport correlations in the two-dimensional turbulent wake. *Phys. Fluids* **26**, 422–427.

HARRIS, V. G., GRAHAM, J. A. & CORRSIN, S. 1977 Further experiments in nearly homogeneous turbulent shear flow. *J. Fluid Mech.* **81**, 657–687.

LARUE, J. C., DEATON, T. & GIBSON, C. H. 1975 Measurement of high frequency turbulent temperature. *Rev. Sci. Instrum.* **46**, 757–762.

LAUNDER, B. E. 1978 Heat and Mass Transport. In *Turbulence* (ed. P. Bradshaw), pp. 232–287. Springer.

LUMLEY, J. L. 1978 Computational modelling of turbulent flows. *Adv. Appl. Mech.* **18**, 123–176.

MEHTA, R. D. & BRADSHAW, P. 1979 Design rules for small low speed wind tunnels. *Aero. J.* **5**, 443–451.

MONIN, A. S. & YAGLOM, A. M. 1971 *Statistical Fluid Mechanics*, vol. 1. MIT Press.

NEWMAN, G. R., LAUNDER, B. E. & LUMLEY, J. L. 1981 Modelling the behaviour of homogeneous scalar turbulence. *J. Fluid Mech.* **111**, 217–232.

POPE, A. & HARPER, J. L. 1966 *Low Speed Wind Tunnel Testing*. Wiley.

RAUPACH, M. R. & LEGG, B. J. 1983 Turbulent dispersion from elevated line source: measurements of wind-concentration moments and budgets. *J. Fluid Mech.* **136**, 111–137.

REYNOLDS, W. C. 1976 Recent advances in the computation of turbulent flows. *Adv. Chem. Engng* **9**, 193–246.

ROHR, J. J., ITSWEIRE, E. C., HELLAND, K. N. & VAN ATTA, C. W. 1988 An investigation of the growth of turbulence in uniform-mean-shear flow. *J. Fluid Mech.* **187**, 1–33.

SAWFORD, B. L. & HUNT, J. C. R. 1986 Effects of turbulence structure, molecular diffusion and source size on scalar fluctuations in homogeneous turbulence. *J. Fluid Mech.* **165**, 373–400.

SHIH, T. & LUMLEY, J. L. 1986 Influence of timescale ratio on scalar flux relaxation: modelling Sirivat & Warhaft's homogeneous passive scalar fluctuations. *J. Fluid Mech.* **162**, 211–222.

SHLIEN, D. J. & CORRSIN, S. 1976 Dispersion measurement in a turbulent boundary layer. *Intl J. Heat Mass Transfer* **19**, 285–295.

SIRIVAT, A. & WARHAFT, Z. 1983 The effect of a passive cross-stream temperature gradient on the evolution of temperature variance and heat flux in grid turbulence. *J. Fluid Mech.* **128**, 323–346.

STAPOUNTZIS, H., SAWFORD, B. L., HUNT, J. C. R. & BRITTER, R. E. 1986 Structure of the temperature field downwind of a line source in grid turbulence. *J. Fluid Mech.* **165**, 401–424.

SUBRAMANIAN, C. S. 1980 Some properties of the larger scale structure in slightly heated turbulent boundary layer. PhD dissertation, University of Newcastle, Australia.

SUBRAMANIAN, C. S. & ANTONIA, R. A. 1981 Effect of Reynolds number on a slightly heated turbulent boundary layer. *Intl J. Heat Mass Transfer* **24**, 1833–1846.

TAVOULARIS, S. & CORRSIN, S. 1981 Experiments in nearly homogeneous turbulent shear-flow with a uniform mean temperature gradient. Part 1. *J. Fluid Mech.* **104**, 311–347.

TENNEKES, H. & LUMLEY, J. L. 1972 *A First Course in Turbulence*. MIT Press.

TOWNSEND, A. A. 1976 *The Structure of Turbulent Shear Flow*, 2nd edn. Cambridge University Press.

WARHAFT, Z. 1980 An experimental study of the effect of uniform strain on thermal fluctuations in grid-generated turbulence. *J. Fluid Mech.* **99**, 545–573.

WARHAFT, Z. 1984 The interference of thermal fields from line sources in grid turbulence. *J. Fluid Mech.* **144**, 363–387.

WARHAFT, Z. & LUMLEY, J. L. 1978 An experimental study of the decay of temperature fluctuations in grid-generated turbulence. *J. Fluid Mech.* **88**, 659–684.

ZEMAN, O. & LUMLEY, J. L. 1979 Buoyancy effects in entraining turbulent boundary layers: a second-order closure study. In *Turbulent Shear Flows*, vol. 1 (ed. E. Durst, B. E. Launder, F. W. Schmidt, J. H. Whitelaw), pp. 295–306. Springer.